Short communication

Ionic resistance of the catalyst layer after the PEM fuel cell suffered freeze

Junbo Hou [a,b], Wei Song [a,b], Hongmei Yu [a,*], Yu Fu [a,b],
Lixing Hao [a,b], Zhigang Shao [a], Baolian Yi [a]

[a] *Fuel Cell System and Engineering Laboratory, Dalian Institute of Chemical Physics,
Chinese Academy of Sciences, 457 Zhongshan Road, Dalian 116023, PR China*
[b] *Graduate University of the Chinese Academy of Sciences, Beijing 100039, PR China*

Abstract

With electrochemical impedance spectroscopy (EIS), the ionic resistances of the catalyst layer (CL) were measured at different current densities after the proton exchange membrane (PEM) fuel cell suffered the subfreezing temperature. Compared with those of the CL before being frozen, the ionic resistances unexpectedly decreased a little, which accorded well with the polarization results. Considering that the frequency-dependent penetration depth was small in the high frequency region, a semi-quantitative method based on the finite transmission-line equivalent circuit was followed to investigate the ionic resistance profile across the whole CL. The results indicated that the change of the ionic resistance profile was not uniform across the CL after the cell experienced freeze/thaw cycles, which was more evident at the higher current densities.
© 2007 Elsevier B.V. All rights reserved.

Keywords: Proton exchange membrane (PEM) fuel cell; Subzero; Freeze/thaw; Electrochemical impedance spectroscopy (EIS); Ionic resistance

1. Introduction

Proton exchange membrane (PEM) fuel cells used for practical transportation applications must be survivable at subzero temperature and capable of cold-starting, and increasing efforts have been put into this subject [1–8]. In the early work of reducing Pt loading and improving cell performance, Nafion® was impregnated in the catalyst layer (CL) to extend the three phase boundaries (TPBs) [9]. In this field, the ionic resistance of the CL plays an important role in the electrode characterization, and it can be measured by the electrochemical impedance spectroscopy (EIS) [10–12]. Unlike the situation at ambient temperature, the influence of water freezing on the electrode quality and the CL structure are not well understood and the investigation on the ionic resistance has not been reported yet.

Based on the agglomerate model, the impedance response of the porous CL can be modeled by the finite transmission-line

equivalent circuit [13]. The impedance behavior of the PEM fuel cell can be described in Fig. 1. This equivalent circuit consists of the membrane resistance (R_m), the electrochemical reaction in the CL and the bulk resistance plus the contact resistance ($R_b + R_c$). The upper rail and the lower rail represent the proton access and electron access in the CL, respectively. The $R_{i,j}$ and the $R_{e,j}$ denote the distributed ionic resistance and the distributed electron resistance, respectively. Usually, the distributed electron resistance can be neglected in the equivalent circuit. The charge transfer process ($R_{ct,j}$) and the dynamic charging process of the double layer (Cd_j) are also included. In the linear polarization regime, the impedance behavior can be depicted as [13]:

$$Z = \sqrt{R_i Z_{ct}} \coth\left(\sqrt{\frac{R_i}{Z_{ct}}}\right) \tag{1}$$

where R_i is the ionic resistance in CL, and Z_{ct} is the CL impedance including the charge transfer process (R_{ct}) and the double layer charging process (Cd). For a finite transmission-line equivalent circuit with n repeating units (Fig. 1), $R_i = n R_{i,j}$,

* Corresponding author. Tel.: +86 411 84379051; fax: +86 411 84379185.
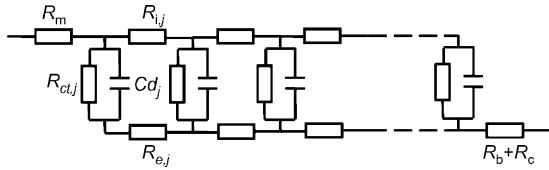*E-mail address:* hmyu@dicp.ac.cn (H. Yu).

Fig. 1. The finite transmission-line equivalent circuit including the double layer and the charge transfer resistance.

$Cd = n\,Cd_j$, $R_{ct} = R_{ct,j}/n$. When H_2/N_2 is used, there is no charge transfer process, and the Z_{ct} can be expressed as:

$$Z_{ct} = \frac{1}{jw\,Cd} \tag{2}$$

where Cd is the double layer capacitance of CL, w the frequency, $j = \sqrt{-1}$. Therefore, R_i can be obtained by fitting the impedance plots to the Eq. (1) and Eq. (2). There exists another method. An asymptotic expansion of Eq. (1) results in [14].

$$Z(w \rightarrow 0) = \frac{R_i}{3} + \frac{1}{jw\,Cd} \tag{3}$$

Hence, $R_i/3$ can be obtained by extrapolating the Nyquist plots in the low frequency region with the real axis [10,11]. When H_2/O_2 is used, the cell impedance behavior still follows the Eq. (1) at the condition of $R_i/R_{ct} \ll 1$ [12]. The Z_{ct} is thus expressed as:

$$Z_{ct} = \frac{R_{ct}}{1 + jw\,R_{ct}\,Cd} \tag{4}$$

where R_{ct} is charge transfer resistance.

In this study, another method based on the frequency-dependent impedance in the high frequency region was followed to measure the ionic resistance of the CL. The cell suffered eight freeze/thaw cycles, and the EIS was carried out along with the measurement of polarization curves. We attempted to investigate whether the ionic resistance of the CL would change after the cell experienced the freeze/thaw cycles, and we further characterized its variation. The results will give some information on the electrode structure.

2. Experimental

2.1. Materials and fabrication

Toray carbon paper, Nafion® solution and PTFE suspension were used to fabricate the gas diffusion electrodes (GDEs). The gas diffusion electrode and N212 membrane were hot-pressed to form the membrane electrode assembly (MEA) with an effective area of $4\,cm^2$ [15].

2.2. Electrochemical characteristics

The cell performance was tested at $60\,°C$. O_2 and H_2 were fed at the out-flow rates of 100 and $40\,ml\,min^{-1}$, respectively. After the I–V plot was recorded, the in situ electrochemical impedance spectroscopy was measured by a KFM2030 impedance meter (Kikusui, Japan). The perturbation amplitude for the sine signal

was $165\,mA$ (peak to peak) over a frequency range from $10\,kHz$ to $0.5\,Hz$.

2.3. Freeze/thaw cycle

The cell was purged by dry gas to remove water, and then operated at $60\,°C$ with humidified reactant gases to obtain $41.6\,mg\,cm^{-2}$ residual water. The cell inlets and outlets were sealed and the cell temperature was kept at $-10\,°C$ for $1.5\,h$. Then, the cell was taken out of the climate chamber, and warmed using hot air provided by air conditioner. When the cell temperature was higher than $10\,°C$, the cell was set on the home-made fuel cell test station and tested at $60\,°C$. This test station had good reproducibility [16]. The procedure was repeated for eight cycles [17].

3. Results and discussion

For the cell before and after freeze, the Nyquist plots at current densities of 0.0025, 0.01, 0.02 and $0.03\,A\,cm^{-2}$ are shown in Fig. 2. As it is shown, the impedance depends strongly on the cathode overpotential [17]. With the increase of current density, the diameter of the arc decreases. The ohmic resistance, the charge transfer resistance and the constant phase element (CPE) can be obtained by nonlinear least-square fitting (NLSF). In the high frequency region, the impedance response represents a Warburg-like straight line at about 45°. This region is dominated by the charging process of the double layer coupled with the proton transport in the CL, and it does not depend on the cathode overpotential.

Since the impedance behavior in the high frequency region is independent on any of approximation, the impedance response can be described as Eq. (4) [13]:

$$Z = \omega^{-1/2}\sqrt{\frac{R_i}{Cd}}\,\frac{\sqrt{2}}{2}(1-j) \tag{5}$$

The frequency-dependent impedance is only determined by the ratio of R_i to Cd. A plot of $|Z|$ as the function of $\omega^{-1/2}$ will give
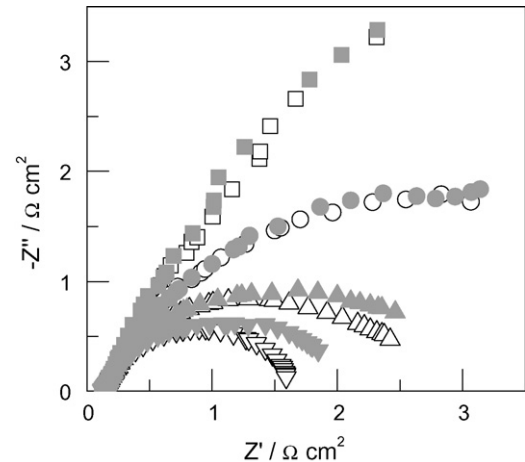

Fig. 2. Nyquist plots for the cell at current densities of 0.0025 (□), 0.01 (○), 0.02 (△) and 0.03 (▽) $A\,cm^{-2}$ before (the hollow) and after (the solid) freeze.
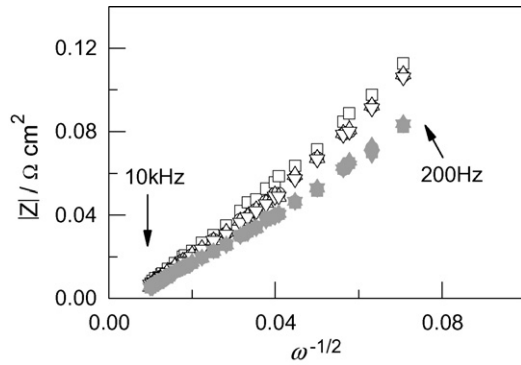
Fig. 3. Plots of R_Ω-corrected $|Z|$ as the function of $\omega^{-1/2}$ for the cell at current densities of 0.0025 ($\square$), 0.01 ($\bigcirc$), 0.02 ($\triangle$) and 0.03 ($\triangledown$) A cm^{-2} before (the hollow) and after (the solid) freeze.

Fig. 4. Plots of capacitance against resistance from the data in Fig. 2 at current densities of 0.0025 ($\square$), 0.01 ($\bigcirc$), 0.02 ($\triangle$) and 0.03 ($\triangledown$) A cm^{-2} before (the hollow) and after (the solid) freeze: (a) ionic resistance profiles across the whole catalyst layer; (b) ionic resistance profiles close to the interface between the membrane and the catalyst layer.

the slope of $(R_i/\mathrm{Cd})^{1/2}$. If the double layer capacitance (Cd) is known or can be calculated by other methods, the ionic resistance of the CL can thus be determined. Hence, the modulus of the impedance ($|Z|$) is corrected by the ohmic resistance (R_Ω), and the plots of R_Ω-corrected $|Z|$ as the function of $\omega^{-1/2}$ are illustrated in Fig. 3. The high frequency region is chosen from the highest frequency (10 kHz) to 200 Hz. The plots of $|Z|$ against $\omega^{-1/2}$ show a linear relationship at the four current densities. The slopes of $(R_i/\mathrm{Cd})^{1/2}$ are thus obtained by linear fitting the data in Fig. 3 and listed in Table 1. The power of each linear fitting is more than 0.99. As theoretically predicted, the slopes of $(R_i/\mathrm{Cd})^{1/2}$ are almost the same at different current densities. And, the slope decreases after the cell suffered freeze.

Instead of another measurement, i.e. cyclic voltammetry (CV) [18], the Cd can be determined by the EIS [19,20]:

$$\mathrm{Cd}^n = \frac{Q}{(R_\Omega^{-1} + R_{ct}^{-1})^{1-n}} \qquad (6)$$

where n is the frequency power, Q the CPE, R_Ω the ohmic resistance, and R_{ct} the charge transfer resistance. The double layer capacitances are thus calculated and listed in Table 1. The values are almost the same as the results of 25 cm^2 MEA [20]. The capacitance decreases slightly with the increase of current density except for the one at 0.0025 A cm^{-2}. At each current density, the capacitance after freeze becomes larger than that before freeze. Since the Cd is obtained by in situ EIS (not by ex situ CV), it can accurately delineate the practical situation of the double layer capacitance when the cell is under operation. The ionic resistances (R_i) can thus be calculated and also summarized in Table 1. Generally, the ionic resistances range from
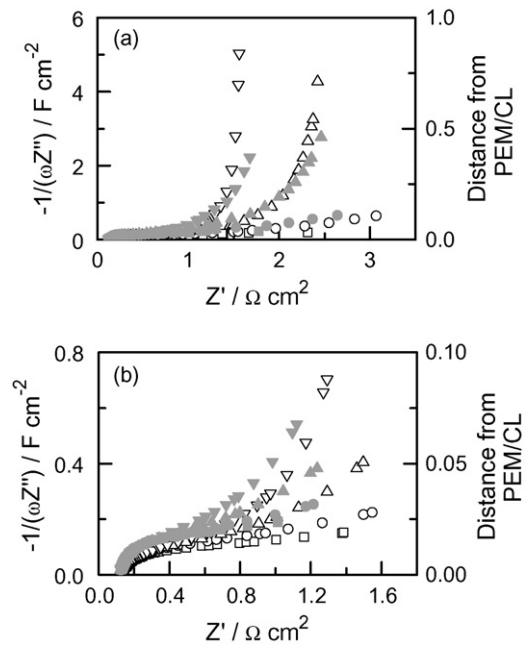
19.2 to 21.0 mΩ cm^2 at the four current densities, and these values are very close to the data from the analytical model and the experimental validation [21]. As the results from the cell operating at relative humidity (RH) 100% [21], the ionic resistance in this study also decreases with increasing current density. Surprisingly, the ionic resistance becomes smaller after the cell experienced eight freeze/thaw cycles.

Considering the fact that the frequency-dependent penetration depth is small in high frequency region [13], it is necessary to investigate the variation of the ionic resistance across the whole CL. The semi-quantitative method [10] is followed here. According to the finite transmission-line equivalent circuit, the ionomer is assumed to distribute homogeneously in the CL. In addition, the distributed capacitances in Fig. 1 are connected in parallel. Hence, the total capacitance increases proportionally to the distance from the interface between the membrane and the CL (PEM/CL). The Nyquist plots in Fig. 2 are transformed to the capacitance plots (Fig. 4a). In essence, the thickness of the catalyst layer that is penetrated can be regarded as a capacitance. There gives a secondary y-axis that schematically depicts

Table 1
Parameters of the electrode quality at different current densities before and after freeze

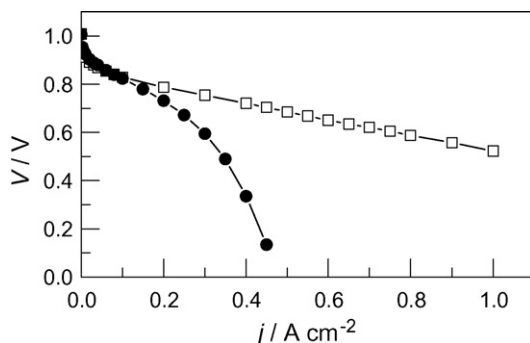| j (A cm^{-2})	$\sqrt{\frac{R_i}{\mathrm{Cd}}}$ (Ω cm^2 s$^{-1/2}$)		Cd (mF cm^{-2})		R_i (mΩ cm^2)		V (V)	
	Before	After	Before	After	Before	After	Before	After
0.0025	1.695	1.225	7.3	11.3	21.0	17.0	0.948	0.954
0.01	1.586	1.238	8.0	11.0	20.1	16.9	0.913	0.924
0.02	1.594	1.255	7.8	10.6	19.8	16.7	0.891	0.903
0.03	1.578	1.226	7.7	10.5	19.2	15.8	0.881	0.889

Fig. 5. The change of polarization for the cell suffered subfreezing temperature: before ($\square$) and after ($\bullet$) freeze.

a depth of penetration in Fig. 4. It is evident that the ionic resistance profiles are different at the four current densities. The higher current density the cell operates at, the more deep the frequency-dependent penetration depth is. Furthermore, beyond a certain distance from the PEM/CL (about $1\,F\,cm^{-2}$), the ionic resistance at 0.02 or $0.03\,A\,cm^{-2}$ increases after the cell experiences freeze/thaw cycles. The ionic resistance profiles close to the PEM/CL are scaled up in Fig. 4b. It is obvious that at the four current densities the ionic resistances decrease after the cell suffers freeze, and this is consistent with the results in Table 1. Since the ionic resistance profiles at 0.0025 and $0.01\,A\,cm^{-2}$ are limited in the region close to the PEM/CL ($<1\,F\,cm^{-2}$), both of them do not behave as those at higher current densities (0.02 and $0.03\,A\,cm^{-2}$). However, the ionic resistances far away from the PEM/CL increase. Since the ionic resistance close to the PEM/CL decreases, the cell performance should be improved at small current densities. The polarization curves before and after the freeze/thaw cycles are shown in Fig. 5, and the voltages at the four current densities are summarized in Table 1. The improved cell performances at small current densities accord well with the decreased ionic resistance close to the PEM/CL. Besides the increased mass transport polarization within the CL [17], the increased ionic resistance far away from the PEM/CL also contributes to the performance loss in high current density region.

4. Conclusions

Based on the electrode impedance behavior in the high frequency region, the ionic resistances were measured at four current densities for a PEM fuel cell experienced eight freeze/thaw cycles. The results showed the ionic resistance decreased with the increase of current density and became smaller within the 10 kHz to 200 Hz penetration depth of the catalyst layer after the cell suffered freeze. This was consistent with the improved cell performance at low current densities. Combined with the semi-quantitative analysis of capacitance against resistance, the change of the ionic resistance profile induced by ice formation was not even across the whole catalyst layer. The ionic resistance close to the interface between the membrane and the catalyst layer decreased, while that away from the interface increased.

References

[1] E.A. Cho, J.-J. Ko, H.-Y. Ha, et al., J. Electrochem. Soc. 151 (2004) A661.
[2] J.S. -Pierre, J. Roberts, K. Colbow, et al., J. New Mat. Electrochem. Syst. 8 (2005) 163.
[3] M. Oszcipok, D. Riemann, U. Kronenwett, et al., J. Power Sources 145 (2005) 407.
[4] Q. Guo, Z. Qi, J. Power Sources 160 (2006) 1269.
[5] J. Hou, H. Yu, S. Zhang, et al., J. Power Sources 162 (2006) 513.
[6] Shanhai Ge, C.-Y. Wang, Electrochem. Solid State Lett. 9 (2006) A499.
[7] L. Mao, C.-Y. Wang, J. Electrochem. Soc. 154 (2007) B139.
[8] K. Tajiri, Y. Tabuchi, F. Kagami, et al., J. Power Sources 165 (2007) 279.
[9] S.J. Lee, S. Mukerjee, J. Mcbreen, Y.W. Rho, Y.T. Kho, T.H. Lee, Electrochim. Acta 43 (1998) 3693.
[10] C. Mark, Lefebvre, Rex B. Martin, Peter G. Pickup, Electrochem. Solid State Lett. 2 (1999) 259.
[11] L. Guangchun, P.G. Pickup, J. Electrochem. Soc. 150 (2003) C745.
[12] R. Makharia, M.F. Mathias, D.R. Baker, J. Electrochem. Soc. 152 (2005) A970.
[13] M. Eikerling, A.A. Kornyshev, J. Electroanal. Chem. 475 (1999) 107.
[14] X. Ren, P.G. Pickup, J. Chem. Soc., Faraday. Trans. 89 (1993) 321.
[15] J. Hou, B. Yi, H. Yu, et al., Int. J. Hydrog. Energy 32 (2007) 4503.
[16] J. Hou, H. Yu, B. Yi, et al., Electrochem. Solid State Lett. 10 (2007) B11.
[17] J. Hou, W. Song, H. Yu, et al., J. Power Sources 171 (2007) 610.
[18] X. Zhao, X. Fan, S. Wang, et al., Int. J. Hydrog. Energy 30 (2005) 1003.
[19] A. Lasia, in: B.E. Conway, J.O.M. Bockris, R.E. White (Eds.), Modern Aspects of Electrochemistry, vol. 32, Plenum, New York, 1999, p. 143.
[20] M. Ciureanu, R. Roberge, J. Phys. Chem. B 105 (2001) 3531.
[21] K.C. Neyerlin, W. Gu, Jacob Jorne, et al., J. Electrochem. Soc. 154 (2007) B279.